Structural characterization of cephaeline binding to the eukaryotic ribosome using Cryo-Electron Microscopy

Kolosova , Olga; Zgadzay, Yury; Stetsenko, Artem; Atamas, Anastasiia; Wu, Cheng-Hsuan; Sachs, Matthew S; Jenner, Lasse; Guskov, Albert; Yusupov, Marat

Published in:
Biopolymers and Cell

DOI:
10.7124/bc.000AA4

Publication date:
2023

ISSN 1993-6842 (on-line); ISSN 0233-7657 (print)
Biopolymers and Cell. 2023. Vol. 39. N 4. P 265–276
http://dx.doi.org/10.7124/bc.000AA4

UDC 577:615.3

Structural characterization of cephaeline binding to the eukaryotic ribosome using Cryo-Electron Microscopy

O. Kolosova[1*], Y. Zgadzay[1*], A. Stetsenko[2], A. Atamas[2], Ch. Wu[3], M. S. Sachs[3], L. Jenner[1], A. Guskov[2], M. Yusupov[1]

[1] Department of Integrated Structural Biology, Institute of Genetics and Molecular and Cellular Biology, University of Strasbourg, Illkirch, 67400, France

[2] Groningen Biomolecular Sciences and Biotechnology Institute (GBB), University of Groningen, Groningen, 9747 AG, the Netherlands

[3] Department of Biology, Texas A&M University; College Station, TX, USA
marat@igbmc.fr, a.guskov@rug.nl

[*] These authors contributed equally to this work.

The eukaryotic ribosome is emerging as a promising target against human pathogens, including amoeba, protozoans, and fungi. Among the eukaryotic-specific families of inhibitors, alkaloids are known to bind to the eukaryotic ribosome and inhibit translocation. However, these inhibitors have varying medical indications and toxicity to humans. Structural information is available for only two of them, cryptopleurine and emetine. **Aim.** In our work, we aimed to elucidate the binding mechanism of another alkaloid, cephaeline, to the eukaryotic ribosome. **Methods.** We used cryogenic electron microscopy and cell-free assays to reveal its mechanism of action. **Results.** Our results indicate that cephaeline binds to the E-tRNA binding site on the small subunit of the eukaryotic ribosome. Similar to emetine, cephaeline forms a stacking interaction with G889 of 18S rRNA and L132 of the protein uS11. We propose the hypothesis of cephaeline specificity to eukaryotes by comparing the interaction pattern of cephaeline with other inhibitors binding to the E-site of the mRNA tunnel. **Conclusions.** The high-resolution structure of ribosome-bound cephaeline (2.45 Å) allowed us to precisely determine the inhibitor's position in the binding site, which holds potential for the development of the next generation of drugs targeting the mRNA tunnel of the ribosome.

K e y w o r d s: Ribosome, cephaeline, anti-protozoan, cryo-EM

Introduction

Given the recent developments in cryogenic electron microscopy (cryo-EM), it is now routinely employed for structure-based drug design, where small changes might be introduced to existing small molecules based on high-resolution structures of the targets. Over 50 % of known antibiotics target the protein synthesis machinery — the ribosome — blocking different translation stages [1, 2]. Moreover, the ribosome is now becoming an important model for structural biology since the resolution of recent ribosome structures is in the range of 1.5-2 Å for cryo-EM [3, 4], and there are structures by X-ray and cryo-electron tomography at high-resolution (≤3 Å) [5–7]. Moreover, the ribosome is becoming the therapeutic target against not only bacteria but also against eukaryotic pathogens, such as protozoans, amoeba, and fungi such as *Candida* spp [8–10].

One of the first discovered anti-protozoan drugs was emetine, extracted from ipecac roots [11]. Nevertheless, emetine is no longer a first-line treatment due to various side effects, especially cardiotoxicity [12]. Later, several synthetic analogs of emetine were developed, such as dehydroemetine, which showed significantly less cardiotoxicity than emetine itself [13]. Another analog of emetine found in similar concentrations in ipecac roots, cephaeline, differs by the absence of a methyl group compared to emetine; however, its spectrum of action appears to be narrower, and it is recommended only for emergency treatment for accidental poisoning [14] and as a potential anti-SARS-CoV-2 agent [15], but is not clinically used as an anti-protozoal treatment.

For a long time, emetine's exact mechanism of action was unknown. Functional studies in Chinese hamster ovary (CHO) cells showed that resistance to emetine is due to the mutation in one of the ribosomal proteins in the small subunit, later identified as S14 (uS11) [16–19], similar to another alkaloid — cryptopleurine [20]. Additionally, a double mutation in the C-terminal part of the uS11 protein affecting R149, and R150 leads to strong emetine resistance [21]. Two decades later, emetine was shown to bind to the E-site on the small subunit of the ribosome [22] and proposed to inhibit protein synthesis by preventing mRNA translocation, similar to cryptopleurine [23]. Nevertheless, structural data are lacking for emetine derivatives such as cephaeline, and thus it has not been possible to relate the binding mechanism with the toxicity and the spectrum of action of these different alkaloids. Moreover, it was unclear why the emetine derivatives such as cryptopleurine are active against eukaryotes, but not against bacteria, unlike the broad-spectrum translation inhibitors pactamycin and amicoumacin A [24–27].

We obtained a high-resolution structure (2.45 Å) of the ribosome-bound cephaeline using single particle cryo-EM. The binding mode of cephaeline was compared with emetine, highlighting the similarity in interaction patterns, and focusing on the more precise determination of the inhibitor position given the high-resolution cryo-EM map. In contrast to emetine, cephaeline binds not only to the E-site on SSU but also to additional areas of the ribosome thought to be structural rather

than functional. Moreover, we compared our structure with several known inhibitors which bind to the E-site on the SSU, highlighting the role of the C-terminal part of the uS11 protein in the eukaryotic specificity for the binding of these alkaloids.

Materials and Methods

Materials

Cephaeline was purchased from Cayman Chemistry and dissolved in 100% EtOH to obtain a 50 mM concentration.

Ribosome purification and crystallization

80S ribosomes from *Candida albicans* were purified as previously described [10].

Cryo-EM complex formation, grid freezing, and image processing

The purified *C. albicans* ribosome sample in buffer G [10 mM Hepes-KOH (pH 7.5), 50 mM KOAc, 10 mM NH_4OAc, 2 mM DTT, and 5 mM $Mg(OAc)_2$] was filtered (0.22 μm centrifugal filters, Millipore) and concentrated to a final concentration of ~1-2 mg ml^{-1}. Cephaeline was added at 1 mM concentration. Aliquots of 2.7 μl were applied to freshly glow-discharged holey carbon grids (Quantifoil Au R1.2/1.3 with 2 nm Ultrathin Carbon support, 300 mesh), and excess liquid was blotted away for 3–5 s with a blotting force set to 1 using an FEI Vitrobot Mark IV (ThermoFisher) and the samples were plunge frozen in liquid ethane. Prepared grids were transferred into Titan Krios 300-keV microscope (Thermo Fisher Scientific), equipped with a K3 direct electron detector. Zero-loss images were recorded semi-automatically using the UCSF Image script [28]. The GIF-quantum energy filter was adjusted to a slit width of 20 eV. Images were collected at nominal magnification, yielding a pixel size of 0.836 Å, with a defocus range of −0.5 to −2.0 μm. Movies were collected with 50 frames dose-fractionated over 2.48 s. We collected 4322 micrographs for the *C. albicans* ribosome in complex with cephaeline.

Motion correction, CTF estimation, manual and template-based particle picking, 2D classification, Ab initio volume generation, CTF global and local refinements, and non-uniform 3D refinement were performed using cryoSPARC (v 4.0) [29]. Maps were sharpened using the Autosharpen Map procedure in Phenix [30]. Using Chimera, the separate masks for the focused refinement were generated for the 60S and 40S subunits. The local resolution map is presented in Figure 1, and the Cryo-EM data processing schemes are presented in Figure 2. Refinement statistics are shown in Table 1.

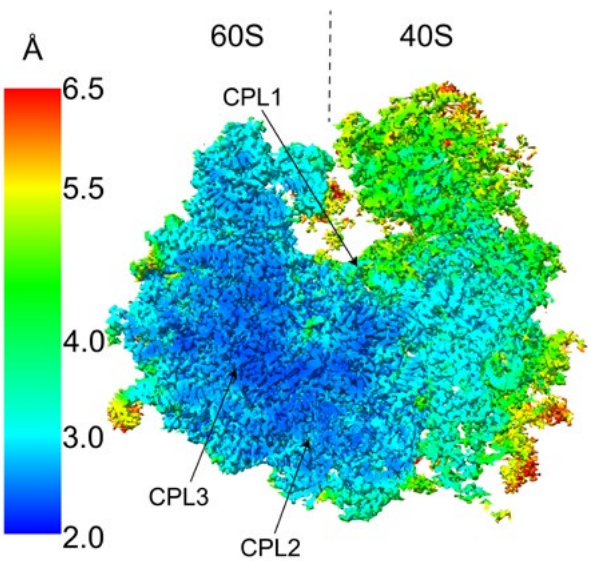

Fig. 1. Local resolution map of the *C. albicans* ribosome in complex with cephaeline.

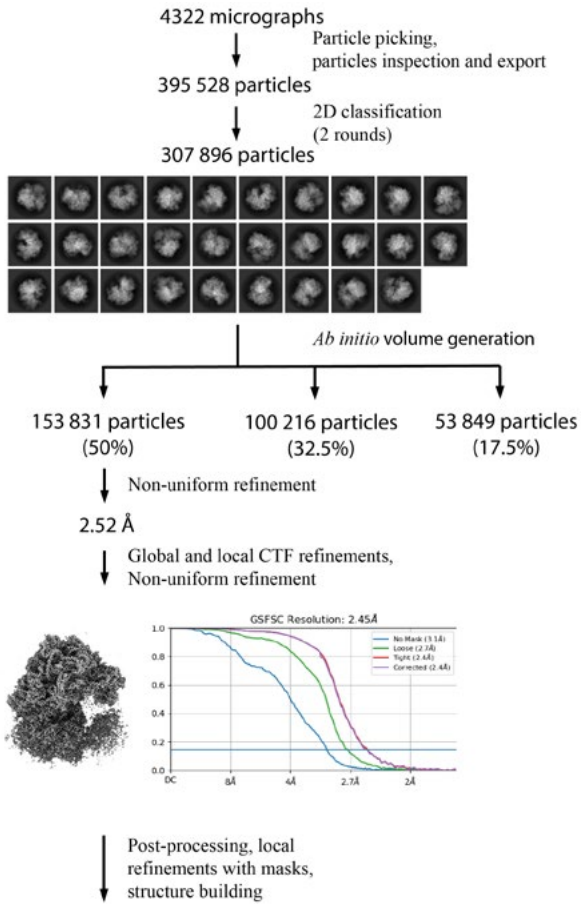

Fig. 2. Cryo-EM data processing scheme for the *C. albicans* ribosome in complex with cephaeline.

Table 1. **Refinement statistics for the 80S *C. albicans* ribosome in complex with cephaeline**

Model	
Chains	78
Atoms	189590
Residues	Protein: 10377 Nucleotide: 4924
Ligands	SPD: 1 ZN: 7 SPK: 1 MG: 367 IAS: 1 YZO: 3
Bonds (RMSD)	
Length (Å) (> 4σ)	0.006 (0)
Angles (°) (> 4σ)	0.745 (35)
MolProbity score	1.45
Clash score	7.23
Ramachandran plot	
Outliers	0.03
Allowed	2.18
Favored	97.79
Rotamer outliers (%)	0.08
Cβ outliers (%)	0.00
Cis proline/general	4.0/0.0
Twisted proline/general	0.0/0.0
CaBLAM outliers (%)	1.18
ADP (B-factors)	
Iso/Aniso (#)	189590/0
Min/max/mean	
Protein	20.48/173.99/60.70
Nucleotide	17.71/237.76/52.37
Ligand	17.24/103.49/35.02
Data	
Box	
Lengths (Å)	247.46, 262.50, 278.39
Angles (°)	90.00, 90.00, 90.00
Supplied Resolution (Å)	2.5
Resolution Estimates (Å)	Masked / Unmasked
d FSC (half maps; 0.143)	2.45 / 3.1
d 99 (full/half1/half2)	2.0/1.7/1.7 / 1.8/1.7/1.7
d model	1.6 / 1.6.3
d FSC model (0/0.143/0.5)	1.6/1.6/2.7 / 1.6/1.7/2.9
Map min/max/mean	-0.33/1.82/0.08
Model vs. Data	
CC (mask)	0.83
CC (box)	0.81
CC (peaks)	0.75
CC (volume)	0.84
Mean CC for ligands	0.62

Inhibition of cell-free translation by cephaeline

The *C. albicans* cell-free experiments were performed in the absence or presence of different concentrations of cephaeline, using methods previously described [10] to characterize other translation inhibitors.

Figure preparation

Cryo-EM maps were manually inspected in Coot [31]. Panels of figures showing structural models were prepared using ChimeraX [32, 33]. The chemical structures were generated using the Marvin ChemAxon package (https://www.chemaxon.com).

Data availability

The cryo-EM model of the ribosome-bound cephaeline and associated maps are deposited to the PDB and Electron Microscopy Data Bank (EMDB) with the following accession codes: PDB ID 8Q5I, EMD-18150, EMD-18151, EMD-18155, EMD-18156.

Results

Cephaeline is the alkaloid, desmethyl analog of emetine, also found in ipecac root. Despite the high similarity to emetine, it was not generally introduced to clinics, and only used in severe poisoning cases to initiate rapid vomiting[14]. Like emetine, cephaeline consists of two rings, benzo[a]quinolizine and isoquinoline, which are connected by a short linker (Fig. 3A). To elucidate the mechanism of action of cephaeline and compare it with other alkaloids, we incubated the 80S ribosome from *C. albicans* in the presence of 1 mM of cephaeline. Subsequently, cryo-EM experiments were performed, resulting in the generation of a high-resolution map (2.45 Å) of the cephaeline-ribosome complex. During map inspection, we found a strong density in E-site on the small subunit, which can be unambiguously assigned to the cephaeline molecule (Fig. 3B).

Cephaeline binds in the E-site pocket, composed of the helices h23, h24, and h45 of 18S rRNA and the protein uS11. Cephaeline replaces the –3 nucleotide of mRNA in the E-site, leading to incorrect mRNA positioning and inhibition translocation (Fig. 3C). Similar to emetine, cephaeline forms several stacking interactions with rRNA and ribosomal proteins. First, there is a benzo[a]quinolizine ring stacking with universally conserved G889 (Fig. 3D). Moreover, the ethyl group of the benzo[a]quinolizine ring forms a C-π interaction with the C991 of the h24 helix. The isoquinoline ring is stacked on the C-terminal residue, L132, of the protein uS11 (Fig. 3E). Apart from the stacking interactions, an additional hydrogen bond is formed between the amide group of the benzo[a]quinolizine ring and the phosphate group of the U1756 of helix h45 (Fig. 3E). Despite the overall similarities in interaction pattern with emetine, our structure is obtained at a higher resolution, resulting in a more precise position of the inhibitor. There is a 1.6 Å difference in the benzo[a] quinolizine ring position and a slight rotation of the isoquinoline ring (Fig. 3F). The only chemical structure difference in cephaeline, namely, the absence of the methyl group in the isoquinoline ring, leaves the remaining hydroxyl group exposed to the solvent region of the mRNA tunnel. Therefore, it is unclear how this difference would impact the observed variations in toxicity and medical indications between emetine and cephaeline that arise

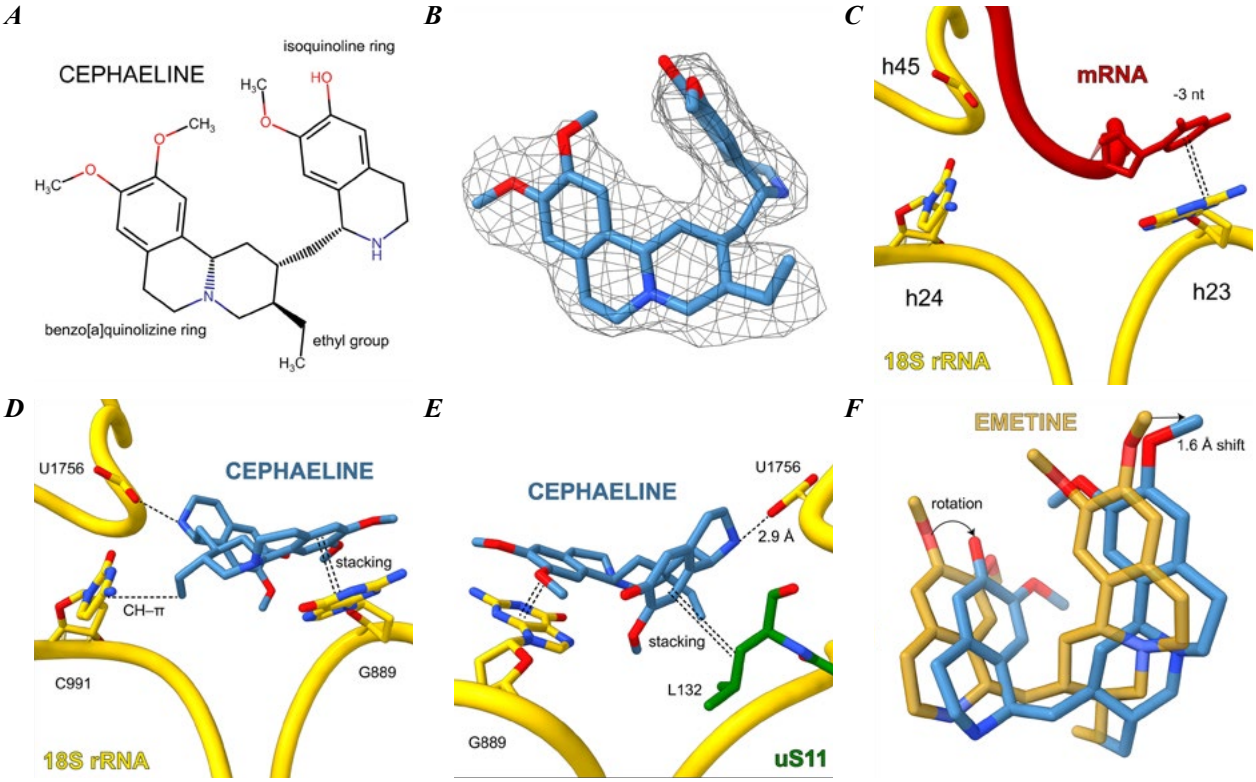

Fig. 3. Cephaeline binds in the E-site on the small subunit (SSU), preventing correct mRNA positioning. *A* — Chemical structure of cephaeline. *B* — Density map of cephaeline bound to the ribosome from *C. albicans* contoured at 3.5σ. *C* — Overview of the E-site on the SSU in *C. albicans*. –3 nucleotide of mRNA stacks onto the G889 base. rRNA is colored in yellow, and mRNA is colored in red. *D* — Cephaeline forms a stacking interaction with G889, CH-π interaction with the C991 base, and a hydrogen bond with U1756. *E* — Cephaeline forms a stacking interaction with the C-terminal residue of the uS11 protein (L132). *F* — Differences between the position of emetine and cephaeline in the E-site on SSU. The emetine molecule was taken from the PDB 6OKK by superimposing the 18S rRNA.

from their interactions with the translational machinery.

The cell-free assays corroborated our results. Translation of sea pansy luciferase (spLUC) in the *C. albicans* cell-free translation extract (CFTS) is sensitive almost at the same level as in CHO extracts [16]. The 50 % inhibition of translation is observed at 1 μM concentration, which indicates the high sensitivity to cephaeline (Fig. 4). The cell-free results suggest that the E-site on the SSU is highly

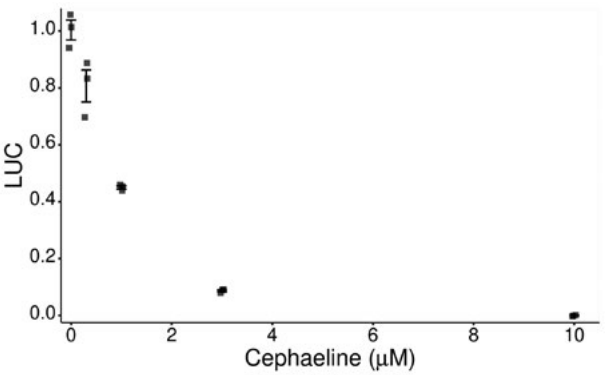

Fig. 4. Inhibition of translation by cephaeline in cell-free translation extracts (CFTSs) from *C. albicans*.

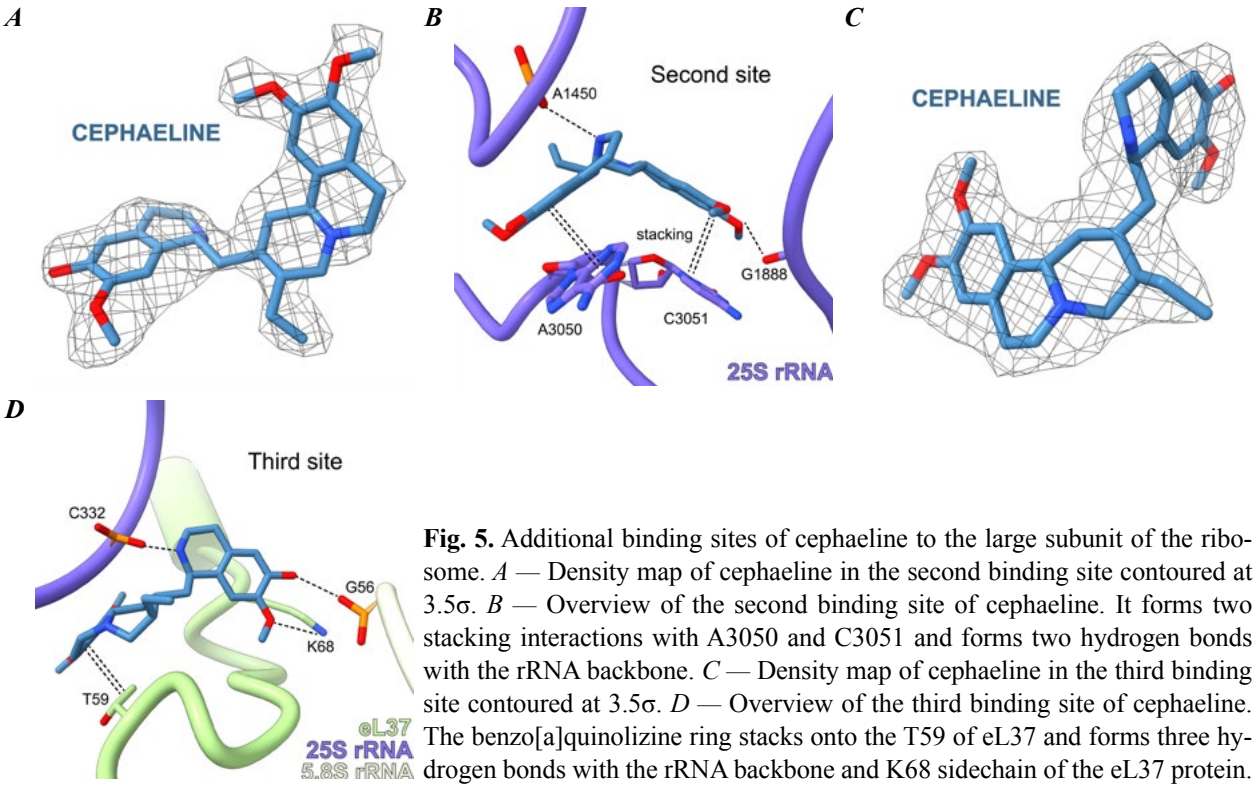

Fig. 5. Additional binding sites of cephaeline to the large subunit of the ribosome. *A* — Density map of cephaeline in the second binding site contoured at 3.5σ. *B* — Overview of the second binding site of cephaeline. It forms two stacking interactions with A3050 and C3051 and forms two hydrogen bonds with the rRNA backbone. *C* — Density map of cephaeline in the third binding site contoured at 3.5σ. *D* — Overview of the third binding site of cephaeline. The benzo[a]quinolizine ring stacks onto the T59 of eL37 and forms three hydrogen bonds with the rRNA backbone and K68 sidechain of the eL37 protein.

conserved across eukaryotes regarding sensitivity to cephaeline.

In addition to the E-site SSU binding, we discovered several additional binding sites for cephaeline in the ribosome distinct from those previously observed for other alkaloids such as emetine. The first additional binding site is in the core of the large subunit (LSU) between the helices H47, H61, and H96. We observed a strong density that can be unambiguously ascribed to a cephaeline molecule (Fig. 5A). Similarly to the previously described the main binding site in the E-site of SSU, cephaeline forms two stacking interactions that stabilize it in the pocket. There is stacking of the benzo[a]quinolizine ring with the A3050 base, and the quinoline ring stacks with the C3051 base (Fig. 5B). Moreover, there are two hydrogen bonds formed with the backbone: the hydroxyl group of the isoquinoline ring interacts with the ribose of G1888, and the amide group of the benzo[a]quinolizine ring interacts with the phosphate group of the A1450 of helix H47 (Fig. 3B). The second additional binding site is also located in the LSU, in-between helix H4 of 25S rRNA, helix H6 of 5.8S rRNA, and the protein eL37, where we observed a strong density for cephaeline molecule (Fig. 5C). The benzo[a]quinolizine ring is restricted by the backbone of protein eL37 (56–61 aas) and the 25S rRNA (328–333 nts). It stacks with the T59 residue of the eL37

protein (Fig. 5D). The isoquinoline ring is placed between the helices H4 and H6. The conformation of the ring is stabilized by the three hydrogen bonds formed: the amide group interacts with the phosphate group of C332, the hydroxyl group interacts with the phosphate group of G56 (5.8S rRNA) and the O-CH_3 group interacts with the NH group of K68 sidechain (eL37 protein, Fig. 5D).

Although alkaloids, such as emetine and cryptopleurine, have been investigated by functional and structural approaches, the mechanisms of their eukaryotic specificity still need to be better understood. Compared with the E-site SSU binding inhibitors of a broad spectrum of action, such as amicoumacin and pactamycin (Fig. 6A), there are distinct differences in the chemical structure. Amicoumacin and pactamycin, which possess a broad spectrum, interact with the G695 by 1/2-ring complexes, while the alkaloids such as cryptopleurine and emetine interact via 3-ring complexes (Fig. 4B). Our high-resolution structure of ribosome-bound cephaeline allowed us to elucidate the complete interaction pattern and describe the specificity of alkaloids to eukaryotes. We assume that emetine derivatives cannot bind to the bacterial ribosome due to the absence of one of the stacking interactions — the isoquinoline ring stacks with the C-terminal L132 of the uS11 protein in eukaryotes. The C-terminal region of this protein is much shorter in bacteria and does not reach the E-site on the SSU (Fig. 6).

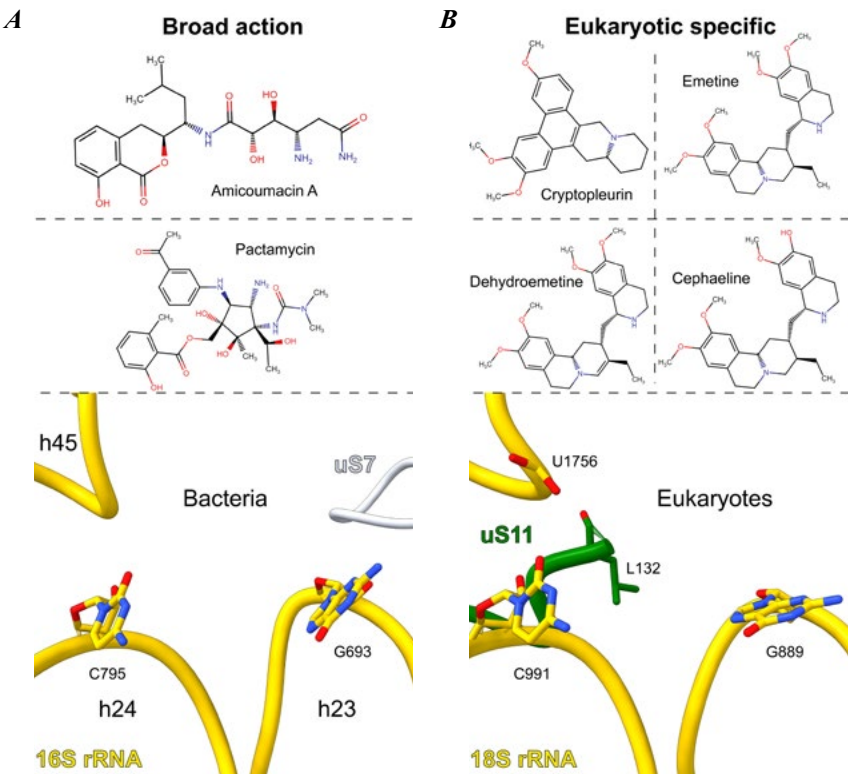

Fig. 6. Comparison of the E-site on the SSU in bacteria and eukaryotes. *A* — Chemical structure of the known E-site SSU inhibitors with the broad-spectrum of action and the composition of the E-site in bacteria. Compared to eukaryotes, the bacteria-specific extension in the uS7 protein forms a restriction of the E-site SSU pocket. *B* — Chemical structure of the known eukaryotic-specific E-site SSU inhibitors and the composition of the E-site in eukaryotes. Compared to bacteria, there is an extension in the C-terminal part of the uS11 protein, stabilizing the emetine derivatives in the pocket by forming a stacking interaction with the isoquinoline ring.

We propose that without the presence of a C-terminal extension, the isoquinoline ring would be flexible, preventing the binding of alkaloids to the E-site in bacteria and defining its eukaryotic specificity, along with the 3-ring complex benzo[a]quinolizine group. On the other hand, the broad-active E-site SSU inhibitors, such as amicoumacin A and pactamycin, do not interact with the uS11 protein. Hence, the presence or absence of this C-terminal extension in the uS11 protein does not affect their binding. Moreover, amicoumacin and pactamycin penetrate more in-between helices h24 and h45, stabilizing the inhibitors in the pocket through the several hydrogen bonds formed with the phosphate backbone. We also suggest that the E-site on the SSU can be utilized for developing new potential antibiotics, considering the presence of a specific bacterial extension in the protein uS7 (Fig. 6A) and the fact that none of the current E-site SSU inhibitors interacts with it.

While the specificity of the E-site SSU inhibitors to the species can be described from the structural point of view, the toxicity and medical indications cannot be explained unequivocally. Emetine, primarily active against protozoans and amoeba, possesses high cardiotoxicity in humans. At the same time, dehydroemetine, which is different only by double bond next to the ethyl group (Fig. 6B), is much less toxic. Cephaeline is not listed as an antiprotozoal inhibitor; nevertheless, the chemical composition is almost identical, and the difference is that there is depletion of the methyl group in the isoquinoline ring, which does not interact with ribosomal proteins/rRNA. If we compare the sequence of the E-site in human and *C. albicans* ribosomes with that in *Plasmodium falciparum* ribosomes, we do not observe any differences between them (Table 2), suggesting that the binding mechanism should be identical in both species. Nevertheless, the structural comparison of the emetine binding to *P. falciparum* and cephaeline binding to *C. albicans* reveals a difference in the position of the benzo[a]quinolizine group (1.6 Å shift) and a slight rotation of the isoquinoline ring. We assume that these observed differences are not due to distinct binding modes of inhibitors but might be somewhat related to the different resolutions achieved (2.45 Å instead of 3.2 Å), as the conformation of neighboring nucleotides remains unchanged. The differences in the toxicity and the medical indication can be related not to the inhibitors binding to the ribosome, but perhaps due to the drug penetration and delivery inside the cell or targeting other biomolecular complexes in the cell.

Conclusion

Using cryo-EM, we obtained a high-resolution structure of the 80S ribosome-bound cephaeline, which allowed us to reveal its mechanism of action. Similar to emetine, cephaeline primarily binds to the E-site on the SSU, forming the stacking interaction with G889 and the L132 of the uS11 protein. However, given the high-resolution structure obtained, we precisely defined the position of the cephaeline molecule, in which the benzo[a]quinolizine group is shifted by 1.6 Å with the slight rotation of the isoquinoline ring compared to emetine. Moreover, cephaeline binds not only to the E-site but also to two additional sites on the LSU, which were not observed before for other alkaloids. By comparing our structure

Table 2. **E-site SSU composition variations across different species**

Site	Molecule name	Residue			
		C. albicans	*H. sapiens*	*P. falciparum*	*T. thermophilus*
E-site SSU	18S (16S) rRNA	U888 (h23)	U960	U972	U692
		G889 (h23)	G961	G973	G693
		A890 (h23)	A962	A974	A694
		A990 (h24)	A1062	A1074	A794
		C991 (h24)	C1063	C1075	C795
		C992 (h24)	C1064	C1076	C796
		U1756 (h45)	U1838	U2061	U1506
	uS11 protein	R130	R149	R149	-
		R131	R150	R150	-
		L132	L151	L151	-
	uS7 protein	-	-	-	G81
		-	-	-	G82
		-	-	-	A83

with other known E-site SSU inhibitors, we propose that emetine derivatives are specific to eukaryotes, highlighting the role of 3-ring benzo[a]quinolizine group and the C-terminal extension in the uS11 protein.

Acknowledgments

Molecular graphics and analyses performed with UCSF ChimeraX, developed by the Resource for Biocomputing, Visualization, and Informatics at the University of California, San Francisco, with support from National Institutes of Health R01-GM129325 and the Office of Cyber Infrastructure and Computational Biology, National Institute of Allergy and Infectious Diseases. We thank Matthew Breuer for help with the figure preparation of cell-free assays.

Funding

This work was supported by Fondation pour la recherche médicale [#FDT202204014886 to O.K.].

REFERENCES

1. *Lin J, Zhou D, Steitz TA, et al., and Gagnon MG. Ribosome-Targeting Antibiotics: Modes of Action, Mechanisms of Resistance, and Implications for Drug Design. Annu Rev Biochem*. 2018; **87**:451–78.
2. *Dmitriev SE, Vladimirov DO, Lashkevich KA.* A Quick Guide to Small-Molecule Inhibitors of Eukaryotic Protein Synthesis. *Biochemistry (Mosc).* 2020; **85**(11):1389–421.
3. *Watson ZL, Ward FR, Méheust R, et al., and Cate JH.* Structure of the bacterial ribosome at 2 Å resolution. *Elife.* 2020; **9**:e60482.
4. *Fromm SA, O'Connor KM, Purdy M, et al., and Mattei S. The translating bacterial ribosome at*

1.55 Å resolution generated by cryo-EM imaging services. *Nat Commun.* 2023; **14**(1):1095.
5. *Xue L, Lenz S, Zimmermann-Kogadeeva M, et al., and Mahamid J.* Visualizing translation dynamics at atomic detail inside a bacterial cell. *Nature.* 2022; **610**(7930):205–11.
6. *Xing H, Taniguchi R, Khusainov I, et al., and Beck M.* Translation dynamics in human cells visualized at high resolution reveal cancer drug action. *Science.* 2023; **381**(6653):70–5.
7. *Ben-Shem A, Garreau de Loubresse N, Melnikov S, et al., and Yusupov M.* The structure of the eukaryotic ribosome at 3.*0 Å resolution. Science.* 2011; **334**(6062):1524–9.
8. *Bansal D, Sehgal R, Chawla Y, et al., and Malla N.* In vitro activity of antiamoebic drugs against clinical isolates of Entamoeba histolytica and Entamoeba dispar. *Ann Clin Microbiol Antimicrob.* 2004; **3**:27.
9. *Matthews H, Usman-Idris M, Khan F, et al., and Nirmalan N.* Drug repositioning as a route to anti-malarial drug discovery: preliminary investigation of the in vitro anti-malarial efficacy of emetine dihydrochloride hydrate. *Malar J.* 2013; **12**:359.
10. *Zgadzay Y, Kolosova O, Stetsenko A, et al., and Yusupov M.* E-site drug specificity of the human pathogen Candida albicans ribosome. *Sci Adv.* 2022; **8**(21):eabn1062.
11. *Lee MR.* Ipecacuanha: the South American vomiting root. *J R Coll Physicians Edinb.* 2008; **38**(4):355–60.
12. *Lemmens-Gruber R, Karkhaneh A, Studenik C, Heistracher P.* Cardiotoxicity of emetine dihydrochloride by calcium channel blockade in isolated preparations and ventricular myocytes of guinea-pig hearts. *Br J Pharmacol.* 1996; **117**(2):377–83.
13. *Panwar P, Burusco KK, Abubaker M, et al., and Gutnov A, Fernández-Álvaro E, Bryce RA, Wilkinson J, Nirmalan N.* Lead Optimization of Dehydroemetine for Repositioned Use in Malaria. *Antimicrob Agents Chemother.* 2020; **64**(4):e01444–19.
14. *Maddison JE, Page SW, Church DB.* Small animal clinical pharmacology.
15. *Ren PX, Shang WJ, Yin WC, et al., and Bai F.* A multi-targeting drug design strategy for identifying potent anti-SARS-CoV-2 inhibitors. *Acta Pharmacol Sin.* 2022; **43**(2):483–93.
16. *Gupta RS, Siminovitch L.* Mutants of CHO cells resistant to the protein synthesis inhibitors, cryptopleurine and tylocrebrine: genetic and biochemical evidence for common site of action of emetine, cryptopleurine, tylocrebine, and tubulosine. *Biochemistry.* 1977; **16**(14):3209–14.
17. *Chang S, Wasmuth JJ.* Construction and characterization of Chinese hamster cell EmtA EmtB double mutants. *Mol Cell Biol.* 1983; **3**(5):761–72.
18. *Chang S, Wasmuth JJ.* Genetic and biochemical distinction among Chinese hamster cell emtA, emtB, and emtC mutants. *Mol Cell Biol.* 1983; **3**(3):429–38.
19. *Rhoads DD, Roufa DJ.* Emetine resistance of Chinese hamster cells: structures of wild-type and mutant ribosomal protein S14 mRNAs. *Mol Cell Biol.* 1985; **5**(7):1655–9.
20. *Grant P, Sánchez L, Jiménez A.* Cryptopleurine resistance: genetic locus for a 40S ribosomal component in Saccharomyces cerevisiae. *J Bacteriol.* 1974; **120**(3):1308–14.
21. *Madjar JJ, Nielsen-Smith K, Frahm M, Roufa DJ.* Emetine resistance in chinese hamster ovary cells is associated with an altered ribosomal protein S14 mRNA. *Proc Natl Acad Sci U S A.* 1982; **79**(4): 1003–7.
22. *Wong W, Bai XC, Brown A, et al., and Scheres SH.* Cryo-EM structure of the Plasmodium falciparum 80S ribosome bound to the anti-protozoan drug emetine. *Elife.* 2014; **3**:e03080.
23. *Bucher K, Skogerson L.* Cryptopleurine--an inhibitor of translocation. *Biochemistry.* 1976; **15**(22): 4755–9.
24. *Brodersen DE, Clemons WM Jr, Carter AP, et al., and Ramakrishnan V.* The structural basis for the action of the antibiotics tetracycline, pactamycin, and hygromycin B on the 30S ribosomal subunit. *Cell.* 2000; **103**(7):1143–54.
25. *Garreau de Loubresse N, Prokhorova I, Holtkamp W, et al., and Yusupov M.* Structural basis for the inhibition of the eukaryotic ribosome. *Nature.* 2014; **513**(7519):517–22.

26. *Polikanov YS, Osterman IA, Szal T, et al., and Sergiev PV.* Amicoumacin a inhibits translation by stabilizing mRNA interaction with the ribosome. *Mol Cell.* 2014; **56**(4):531–40.
27. *Prokhorova IV, Akulich KA, Makeeva DS, et al., and Dmitriev SE.* Amicoumacin A induces cancer cell death by targeting the eukaryotic ribosome. *Sci Rep.* 2016; **6**:27720.
28. *Li X, Zheng S, Agard DA, Cheng Y.* Asynchronous data acquisition and on-the-fly analysis of dose fractionated cryoEM images by UCSFImage. *J Struct Biol.* 2015; **192**(2):174–8.
29. *Punjani A, Rubinstein JL, Fleet DJ, Brubaker MA.* cryoSPARC: algorithms for rapid unsupervised cryo-EM structure determination. *Nat Methods.* 2017; **14**(3):290–6.
30. *Liebschner D, Afonine PV, Baker ML, et al., and Adams PD.* Macromolecular structure determination using X-rays, neutrons and electrons: recent developments in Phenix. *Acta Crystallogr D Struct Biol.* 2019; **75**(Pt 10):861–77.
31. *Emsley P, Lohkamp B, Scott WG, Cowtan K.* Features and development of Coot. *Acta Crystallogr D Biol Crystallogr.* 2010; **66**(Pt 4):486–501.
32. *Goddard TD, Huang CC, Meng EC, et al., and Ferrin TE.* UCSF ChimeraX: Meeting modern challenges in visualization and analysis. *Protein Sci.* 2018; **27**(1):14–25.
33. *Pettersen EF, Goddard TD, Huang CC, et al., and Ferrin TE.* UCSF ChimeraX: Structure visualization for researchers, educators, and developers. *Protein Sci.* 2021; **30**(1):70–82.

Вивчення структурних характеристик зв'язування цефаеліну з еукаріотичною рибосомою за допомогою кріоелектронної мікроскопії

О. Колосова, Ю. Згадзай, А. Стеценко, А. Атамась, Ченг Ву, М. С. Сакс, Л. Дженнер, А. Гуськов, М. Юсупов

Еукаріотична рибосома стає перспективною мішенню проти патогенів людини включаючи амеб, протозоїдів та грибів. Серед специфічних для еукаріотів родин інгібіторів відомо, що алкалоїди здатні зв'язуватися з еукаріотичною рибосомою та гальмувати транслокацію. Проте ці інгібітори мають різні медичні показання та токсичність для людини. Структурна інформація доступна лише для двох з них — криптоплеурину та еметину. **Мета.** У нашій роботі ми мали на меті розкрити механізм зв'язування алкалоїду цефаеліну з еукаріотичною рибосомою. **Методи.** Ми використали кріогенну електронну мікроскопію та безклітинну систему трансляції для розкриття механізму його дії. **Результати.** Наші результати свідчать про те, що цефаелін зв'язується з Е-сайтом на малій субодиниці еукаріотичної рибосоми. Подібно до еметину, цефаелін має стекінгову взаємодію з гуаніном G889 18S рРНК та лейцином 132 білка uS11. Ми пропонуємо гіпотезу про специфічність цефаеліну до еукаріотів, порівнюючи патерн взаємодії цефаеліну з іншими інгібіторами, які зв'язуються з Е-сайтом мРНК каналу рибосоми. **Висновки.** Отримана нами структура рибосоми високої роздільної здатності у комплексі з цефаеліном (2,45 Å) дозволила точно визначити позицію інгібітора в місці зв'язування, що може сприяти розробці наступного покоління препаратів, націлених на мРНК канал рибосоми.

Received 09.08.2023